Dynamics of cosmological models with time varying parameters

Chingtham Sonia[1], S. Surendra Singh[2], Angelica Laishram[2],
Md Khurshid Alam[3] and Th. Revekson Singh[1]

[1] Department of Mathematics, D. M. College of Arts, Dhanamanjuri University, Imphal, 795001, India

[2] Department of Mathematics, National Institute of Technology Manipur, Imphal, 795004, India

[3] Department of Mathematics, St. Joseph University, Virgin Town-797115, Nagaland, India

chingtham.sonia19@gmail.com, ssuren.mu@gmail.com, angelicalaishram@gmail.com, alamkhursid96@gmail.com and reveksonthokchom17@gmail.com

(Submitted on 6 April 2025; Accepted on 28 May 2025)

Abstract.

The present paper studies the dynamics of the Friedmann-Lemaître -Robertson-Walker (FLRW) cosmological model with a decaying vacuum energy density Λ in the presence of an arbitrary spatial curvature k. Here, we consider three models: Model I-$G = constant$, $\rho_\Lambda = constant$, Model II: $\dot{G} \neq 0$, $\rho_\Lambda = constant$, Model III-$\dot{G} \neq 0$, $\dot{\rho_\Lambda} \neq 0$. We take Λ as a function of Hubble parameter H. In Model II since matter is not conserved here, we propose an empirical expression of ρ_m to be $\rho_m = \frac{f(t)\rho_o a_o^3}{a^3}$. Also in Model III, since $\dot{G} \neq 0$, G does not remain constant here. So, we consider that G varies with time through H through the following relation: $G = G_o H^{(-1/m)}$, where G_o,$m \in \mathbb{R}$ and $m > 0$. The use of these expressions benefit us in expressing various cosmological parameters in terms of redshift value z_r. In the recent years, analysing cosmological parameters graphically with respect to change in redshift z_r has become a vital matter in studying dynamics of the Universe in modern cosmology. Here, we set up the dynamical system out of the field equations by introducing new set of variables for each of the models and analyze the stability of the developed system in each of the models. We find out the fixed points of the system in finite phase plane as well as analysis of stability of fixed points at infinity using Poincaré sphere. The perturbation plots for each of the axes are presented and the values of cosmological parameters have been estimated for each of the models. In Cosmological parameters such as the equation of state parameter for dark energy sector ω_{de}, total density parameter Ω_{total}, the Hubble parameter H and the deceleration parameter q are obtained as functions of redshift z_r and their plots over redshifts are also provided. From the plot of q with respect to Θ, we find the value of transition redshift z_{rt}. The present values of the above parameters are estimated and they are in agreement with the observational data. For each of the models, we present the testing of the model's parameter space for the present values of H, q, the transition redshift z_{rt} and ω_{de} for testing the significance of the discrepancy between the theoretically calculated value and the observational data. It is found that all the cosmological models developed in spacetimes of arbitrary spacial curvature support the accelerated expansion phenomena of the evolving Universe.

Key words: Dynamical system, fixed points, Poincaré sphere, transition redshift.

Introduction

General Relativity (GR) is one of the most prominent theories that successfully describes the dynamics of the Universe. The discovery of the current accelerated expansion model of the Universe in the last decades is one of the successful achievements of modern observational cosmology [10, 52]. This accelerating behavior of the evolving Universe has been supported by several other cosmological observations [2, 7, 11, 43, 58, 59]. Motivated by Dirac's large number hypothesis in the thirties, the idea of varying gravitational constant G that evolves with time was suggested and to accommodate this varying G

extensions were being made in GR [5, 33, 37, 38]. This idea was also disputed by Teller [14] which was further qualified by Dicke [39, 40]. Many researchers have given immense contributions to explain the accelerated expansion phenomena by putting forward other alternative theories. The Dark energy model is one such model that provides the notion of negative pressure by introducing a cosmological constant Λ in Einstein's equations of General Relativity (GR) [41]. Also, we can mention the successful works in [15, 45, 47–49, 57] based on modified gravity theory which aims at modifying the geometry of spacetime. Further, various aspects and prominent ideas on modified gravity theories from different directions have been considered in [1, 50]. Lima and Maia have also investigated on a phenomenological decay law for Λ in the framework of a flat Friedmann-Robertson-Walker (FRW) geometry [21]. Later Lima and Trodden extended the main results of their previous work [21] in the presence of arbitrary spatial curvature [22]. In [13], they have also analyzed the curved Universe in a separate section. In a successful attempt to portray a complete cosmological scenario including curvature effects in decaying vacuum inflationary cosmologies [23], it is mentioned that the possibility of curvature still deserves a closer scrutiny and also it is interesting to investigate what happens when flat condition is relaxed in a more general treatment. A detail explanation on the merits of proposing a large class of nonsingular cosmologies in solving several cosmological puzzles like the "graceful exit" problem, the cosmological constant problem, etc, has been given in [24] where they focus on the CMB entropy content generated by $\Lambda(H)$ nonsingular cosmology. In the recent years, using new theoretical techniques such as renormalization group (RG) from the side of quantum field theory in curved spacetimes together with the usual phenomenological approach, a large class of dynamical $\Lambda(H)$ models involving even power series of H has been proposed [19, 20, 27].

Motivated by the above studies made on $\Lambda(H)$ cosmology in arbitrary curvature k, the present paper focus on the dynamics of the Friedmann-Lemaître -Robertson-Walker(FLRW) cosmological model with a running cosmological constant Λ in spacetimes of arbitrary spatial curvature k in which we aim to extend the system to a higher dimension in a more generalized way and study the dynamics of the resulting model. Assuming that Λ evolves in power series of H, we aim to set up a dynamical system by using the cosmological field equations and a newly introduced set of variables. We analyze the stability of the developed dynamical system and their cosmological implications in the evolving Universe. Various cosmological parameters have been evaluated along with the respective graphical analysis to explain the accelerated expansion epoch of the present Universe. The discrepancy between the evaluated and the observational data has also been studied by comparing the evaluated values of parameters with the known values in observational data. We arrange the paper in the following way. In section 2, we show the setting up of dynamical system equations from the cosmological field equations and the stability analysis in three subsections that comprise of Model I-$G = constant$ and ρ_Λ =constant, Model II-$\dot{G} \neq 0$, ρ_Λ =constant and Model III-$\dot{G} \neq 0$, $\dot{\rho_\Lambda} \neq 0$. Cosmological parameters have been evaluated in order to perform deep analysis of the physical interpretations and cosmological implications associated with them in each of the subsections. In section 3, we show the testing of model's parameter space for each of the three models. In section 4, we give the conclusion to our study with the corresponding cosmological implications of our theoretical findings.

1 Setting up of dynamical system equations and stability analysis

Let us consider the following Einstein field equations (EFE) in the presence of cosmological constant Λ:

$$R_{\mu\nu} - \frac{1}{2}g_{\mu\nu}R = 8\pi G\mathbf{T}_{\mu\nu}, \tag{1}$$

where $T_{\mu\nu}$ is the ordinary energy-momentum tensor and $\mathbf{T}_{\mu\nu} \equiv T_{\mu\nu} + g_{\mu\nu}\rho_\Lambda$ is the modified energy-momentum tensor. We have assumed the Universe to be filled with a perfect fluid with U_μ as four-velocity vector field and the above EFE describes the effective vacuum contribution with energy density $\rho_\Lambda = \frac{\Lambda}{(8\pi G)}$ with the associated pressure as $p_\Lambda = \omega_{de}\rho_\Lambda$ where $\omega_{de} \to -1$. Here we denote the density of matter-radiation by ρ_m and the corresponding pressure by $p_m = (\gamma-1)\rho_m$. We use the expression $\mathbf{T} = -p_t g_{\mu\nu} + (\rho_t + p_t)U_\mu U_\nu$ to describe the modified energy-momentum tensor where $p_t = p_m + p_\Lambda$ and $\rho_t = \rho_m + \rho_\Lambda$.

Using metrics described by the FLRW line element in the presence of a curvature parameter [21, 26, 28, 53], the EFE can be written as follows:

$$8\pi G\rho_t \equiv 8\pi G\rho_m + \Lambda = 3H^2 + \frac{3k}{a^2}, \tag{2}$$

$$8\pi G p_t \equiv 8\pi G p_m - \Lambda = -2\dot{H} - 3H^2 - \frac{k}{a^2}, \tag{3}$$

where the overhead dot denotes the derivative with respect to the cosmic time t.

Taking into account the general Bianchi identity $\nabla^\mu G_{\mu\nu} = 0$ and using the field equation (1), we consider the following relations:

$$\nabla^\mu(\mathbf{T}_{\mu\nu}) = \nabla^\mu[G(T_{\mu\nu} + g_{\mu\nu}\rho_\Lambda)] = 0.$$

So we have the following mixed local conservation law [17]:

$$\frac{d}{dt}[G(\rho_m + \rho_\Lambda)] + 3GH(\rho_m + p_m) = 0. \tag{4}$$

Taking motivation from the work of Aleksander Stachowski *et* al. [3], we consider the following form of $\Lambda(H)$:

$$\Lambda(H) = \sum_{n=0}^{\infty} \frac{1}{2n!}\frac{d^{2n}}{dH^{2n}}\Lambda(H)|_0 H^{2n}$$
$$\Rightarrow \Lambda(H) = \Lambda_o + \alpha_2 H^2 + \alpha_4 H^4 + ... \tag{5}$$

where $\Lambda_0 = \Lambda(H)|_0$ and α_{2n} $'$s are the coefficients in the Taylor series expansion of $\Lambda(H)$ given by $\alpha_{2n} = \frac{1}{2n!}\frac{d^{2n}\Lambda(H)}{dH^{2n}}|_0$, where $n = 1, 2, ...$

The above form of $\Lambda(H)$ has been discussed in [6]. The dynamical systems approach has also been used for qualitative study of various cosmological models in [44,55,56]. A detailed explanation regarding the contribution of only the even powers of H can be seen from [12,18–20,25,30,51,54]. In order to study the behavior of both the early and the late cosmos in a single unified framework [16,17,25,51], we consider only the terms containing $H^{2n}, n = 1, 2$ beyond the term Λ_o.

Now, using (5) in (3), we obtain the following relations:

$$-2\dot{H} - 3H^2\frac{k}{a^2} = 8\pi G(\gamma - 1)\,\rho_m - \Lambda_0 - \alpha_2 H^2 - \alpha_4 H^4 - ...,$$
$$\Rightarrow 2\dot{H} = \Lambda_0 + (\alpha_2 - 3)H^2 + \alpha_4 H^4 + ... - \frac{k}{a^2} - 8\pi G(\gamma - 1)\rho_m, \quad (6)$$

1.1 Model I- $G = constant$, $\rho_\Lambda = constant$

If both G and ρ_Λ are taken to be constants and if there are no other components in the cosmic fluid, then matter is covariantly self-conserved and it evolves according to the local covariant conservation law of matter-radiation [17] as follows:

$$\dot{\rho_m} + 3\gamma H\rho_m = 0. \quad (7)$$

Let us introduce new variables x, y and z so as to construct the dynamical system such that $x = H^2$, $y = 8\pi G\rho_m$ and $z = \frac{3k}{a^2}$. The variable z denotes the usual z-coordinate measured along the three dimensional z-axis while z_r used in the subsequent analysis denotes the redshift parameter. We substitute $b = 4\pi G\rho_\Lambda$ for our convenience. Using these new variables, namely, x, y and z with equations (2), (3), (6) and (7), we obtain the following autonomous system of ordinary differential equations ($ASODE$) to represent the dynamical system:

$$x' = \frac{2}{3}xz - \gamma y, \quad (8)$$
$$y' = -3\gamma y, \quad (9)$$
$$z' = -2z + \frac{\gamma yz}{x} - \frac{2}{3}z^2. \quad (10)$$

Here, the overhead dash denotes derivative with respect to logarithmic time Θ. Using the above dynamical system equations and relation (2), we get $f_1(\frac{2}{3}b, 0, 0)$ as a fixed point of the above system. We take $z \neq -3$ to analyze stability in the finite phase plane. The Jacobian matrix J at f_1 is given by:

$$J_{f_1} = \begin{pmatrix} 0 & -\gamma & \frac{4b}{9} \\ 0 & -3\gamma & 0 \\ 0 & 0 & -2 \end{pmatrix}.$$

The eigenvalues of J_{f_1} are 0, -3γ and -2. The fixed point f_1 is non-hyperbolic for any γ. So, let us study the behavior of perturbation functions along x, y and z axes. For this, we perturb the system by a small amount and let η_x, η_y and η_z represent the perturbation along the x-axis, $y-$axis and $z-$axis respectively. Then using equations (8), (9) and (10), we obtain,

$$\left.\begin{aligned} \eta_x &= c_o, \\ \eta_y &= c_1 e^{-3\gamma\Theta}, \\ \eta_z &= c_2 e^{-2\gamma\Theta}, \end{aligned}\right\} \tag{11}$$

where c_o, c_1 and c_2 are arbitrary constants of integration. It is graphically shown in Fig. 1 that the perturbations along the y and z axes decay to zero as $\Theta \to \infty$ while η_x evolves to a constant value c_o. This means f_1 is a stable fixed point [34].

Now, in order to analyze the cosmological implications associated with this model, namely, Model I, we obtain the expressions of the following cosmological parameters as follows:

Equation of state for dark energy sector, ω_{de}:

$$\omega_{de} = \frac{-(z+3)x + y}{\Lambda_o + \alpha_2 x + \alpha_4 x^2},$$

The total density parameter, Ω_{total}:

$$\Omega_{total} = \Omega_\Lambda + \Omega_m = \frac{z}{3} + 1.$$

In terms of redshift parameter, z_r with the redshift function $a(t) = \frac{1}{1+z_r}$, we get,

$$\omega_{de} = \frac{-(3 + \frac{3k(1+z_r)^2}{(c_3 + c_4 \ln \frac{1}{1+z_r})^{\frac{2}{3}}}) \left(c_3 + c_4 \ln \frac{1}{1+z_r}\right)^{\frac{2}{3}} + c_5 (1+z_r)^{3\gamma}}{\Lambda_o + \alpha_2 (c_3 + c_4 \ln \frac{1}{1+z_r})^{\frac{2}{3}} + \alpha_4 (c_3 + c_4 \ln \frac{1}{1+z_r})^{\frac{4}{3}}}, \tag{12}$$

$$\Omega_{total} = 1 + \frac{k(1+z_r)^2}{(c_3 + c_4 \ln \frac{1}{1+z_r})^{\frac{2}{3}}}. \tag{13}$$

The Hubble parameter, H is evaluated as follows:

$$H = c_1^{\frac{1}{2}} (\ln \frac{c_2}{(1+z_r)})^{\frac{1}{3}}, \tag{14}$$

where c_1 and c_2 are arbitrary constants of integration. The deceleration parameter, q is obtained as follows:

$$q = \frac{(1+z_r)}{3 \ln \frac{c_2}{(1+z_r)}} - 1\,. \tag{15}$$

The value of the transition redshift, z_{rt} can be obtained as follows:

$$z_{rt} = \{z_r : q_{z_r} = 0\}. \tag{16}$$

The fixed points and their stability nature is shown in Table 1. It is well known that the deceleration parameter determines the accelerating or decelerating behavior while the Hubble parameter decides the rate of expansion of the Universe. So, we analyze the behavior of $H(z_r), q(z_r)$ with respect to z_r by plotting the values of these parameters individually against z_r. This geometrical analysis allows us to study the late time behaviors of the evolving Universe and the associated cosmological implications. Also, we can note down the present values of the above parameters from the respective plot which will be given by the ordinate of that point where the curve meets the vertical axis. The present values of H, q, ω_{de} and z_{rt} are noted in Table. 2. As seen from the plot shown in Fig. 5, the Hubble parameter is a monotonically decreasing function of z_r and it increases with the decrease in z_r. At late time when z_r tends to -1, the value of H tends to infinity which indicates that the rate of expansion becomes infinite at late time. We again observe from Fig. 6 that the deceleration parameter q decreases monotonically with the decrease in redshift value. The negative value of the deceleration parameter, q signifies that there is accelerated expansion in the model universe. From this plot of q, we see that the transition from the early decelerated regime $q(z_r) > 0$ (corresponding to $(z_r > z_{rt})$), into the current accelerated one $q(z_r < 0)$ (corresponding to $(z_r < z_{rt})$) occurs at $z_{rt} = 0.721$. For Model I, the value of z_{rt} remains very close to observational data [35]. The plot of ω_{de} with respect to z_r shown in Fig. 7 helps us to analyze the phantom-like or quintessence-like behavior at late time when the value of z_r tends to -1. In this model, ω_{de} evolves within the phantom regime and at present time when z_r tends to zero from the right, ω_{de} tends to -1 from the left of -1, that is, $\omega_{de} < -1$. This shows that Model I exhibits effective phantom behavior at present with $\omega_{de}(z_{ro}) \simeq -1.02$ which is compatible with observational data [35]. Hence, Model I supports the accelerated expansion phenomena of the evolving Universe.

1.2 Model II- $\dot{G} \neq 0$, $\rho_\Lambda = constant$

Since $\dot{G} \neq 0, G$ does not remain constant here which indicates non-conservation of matter [17]. As ρ_Λ is constant, the relation (4) leads to the following equation:

$$\dot{G}(\rho_m + \rho_\Lambda) + G[\dot{\rho_m} + 3H(\rho_m + p_m)] = 0. \tag{17}$$

Since matter is not conserved here, let us propose the following empirical expression [36]:

$$\rho_m = \frac{f(t)\rho_o a_o^3}{a^3}, \tag{18}$$

where the expression $f(t) = \exp[n(\ln H - \ln H_o)]$ determines how much the expansion rate has changed from its initial rate H_o at any given time t. Here, a_o, H_o and ρ_o denote the values of scale factor, Hubble parameter and matter

density respectively at present time. The parameter n in the expression of $f(t)$ determines how rapidly the expansion rate changes with time. The expression of ρ_m in equation (18) describes the evolution of the universe's density providing a framework to explain cosmological phenomena that can describe the distribution and evolution of matter within the universe's spacetime. For instance, $n = 1$ in the expression of $f(t)$ indicates the universe expanding with constant density, $n > 1$ indicates the universe where the expansion rate is slowing down faster than the matter-dominated universe and $n < 1$ indicates the universe where the expansion rate is slowing down, slower than in a matter-dominated universe. The use of this expression of ρ_m also benefits us in finding various important cosmological parameters in terms of redshift z_r which is a very essential part for understanding the dynamics and evolution of the cosmos. Expressing in terms of redshift z_r independent of the variables x, y and z represents a distinct aspect of the cosmological model by allowing us to analyze graphically the dynamical behavior of the Universe in a more efficient way within a small range of z_r value, that is, $z_r \in [-1, 1]$.

Now, we consider new variables: $x = \frac{8\pi G}{3H^2}$, $y = \rho_m$ and $z = \frac{k}{H^2a^2}$ to set up the dynamical system. Using these, (6) can now be expressed in terms of x, y and z as follows:

$$\dot{H} = \frac{3H^2}{2}(\frac{2z}{3} - \gamma xy). \tag{19}$$

Using (19) and the newly introduced variables in the above field equations, we obtain the following $ASODE$ which will represent the dynamical system:

$$x' = \frac{dx}{d\Theta} = \dot{x}\frac{dt}{d\Theta}$$

$$x' = \frac{-nxyz}{y + \rho_\Lambda} + \frac{3\gamma n x^2 y^2}{2(y + \rho_\Lambda)} - \frac{3\gamma(\gamma - 1)xy}{y + \rho_\Lambda} - 2xz + 3\gamma x^2 y, \tag{20}$$

where $\Theta = \ln a$ denotes the logarithmic time with respect to the scale factor a. The overhead dash denotes the derivative with respect to Θ while the overhead dot denotes the derivative with respect to cosmic time t. Similarly, we get

$$y' = nyz - \frac{3\gamma n x y^2}{2} - 3y, \tag{21}$$

$$z' = -2z^2 + 3\gamma xyz - 2z. \tag{22}$$

From the above system, we obtain the following three fixed points: $F_1(0, 0, 0)$, $F_2(\frac{1}{\rho_\Lambda}, 0, 0)$ and $F_3(0, 0, -1)$. However, we will not consider F_3 as this fixed point is not physically feasible. To analyze the stability of the fixed points, we will find the Jacobian matrix (J) at the respective fixed points.

Now, the Jacobian matrix at the fixed point F_1 is given by

$$J_{F_1} = \begin{pmatrix} 0 & 0 & 0 \\ 0 & -3 & 0 \\ 0 & 0 & -2 \end{pmatrix},$$

$$J_{F_2} = \begin{pmatrix} 0 & \frac{3\gamma^2}{\rho_\Lambda^2} & \frac{-2}{\rho_\Lambda} \\ 0 & -3 & 0 \\ 0 & 0 & -2 \end{pmatrix}.$$

J_{F_1} is a diagonal matrix and J_{F_2} is a triangular matrix whose eigenvalues are given by the diagonal entries. So, the eigenvalues of J_{F_1} and J_{F_2} are the same, namely $(0, -3, -2)$. Both F_1 and F_2 are non-hyperbolic fixed points as one of the eigenvalues vanishes. As they are non-hyperbolic, we cannot use linear stability theory. Instead, we need to find the perturbation functions along the x, y and z axes, we analyze their nature with respect to Θ. In a three dimensional dynamical system, we can analyze stability of non-hyperbolic fixed points by analyzing the nature of perturbation along each of the axes [56].

Now let us find the perturbation functions at F_1 and F_2 as functions of logarithmic time Θ. Now, we perturb the system by a small amount, $x = \eta_x$, $y = \eta_y$ and $z = \eta_z$ where η_x, η_y and η_z represent small perturbations along x, y and z axes respectively. With these perturbed system using (20), (21) and (22), we obtain the following expressions of the perturbation functions at both F_1 and F_2:

$$\begin{aligned} \eta_x &= d_{oo} \\ \eta_y &= d_{o1} \exp(-3\Theta) \\ \eta_z &= d_{o2} \exp(-2\Theta), \end{aligned}$$

where d_{oo}, d_{o1} and d_{o2} are arbitrary constants of integration.

In Fig. 2, it can be seen that the perturbation along x-axis, η_x evolves to a constant value when Θ tends to infinity while both η_y and η_z, being monotone decreasing functions of Θ, gradually decrease as Θ increases and finally decay to zero as Θ tends to infinity. So, we can conclude that F_1 and F_2 are stable fixed points. Since the non-vanishing eigenvalues of J_{F_1} and J_{F_2} are all negative and also as F_1, F_2 are stable fixed points from perturbation function approach, we can conclude that at late time, F_1 and F_2 represent stable attractors. The presence of the late time attractors in the system assure the presence of negative pressure representing the accelerated expansion phase of the evolving Universe.

To analyze stability at infinity in the infinite phase plane, we need to extend the above rectangular coordinates to the Poincaré sphere S^3 [42]. Through stereographic projection, the upper hemisphere of S^3 is projected onto $\mathbf{R}^3$ by transforming the coordinates as $x = \frac{X}{W}$, $y = \frac{Y}{W}$, $z = \frac{Z}{W}$ and $X = \frac{x}{\sqrt{1+|\mathbf{x}|^2}}$, $Y = \frac{y}{\sqrt{1+|\mathbf{x}|^2}}$, $Z = \frac{z}{\sqrt{1+|\mathbf{x}|^2}}$ and $W = \frac{1}{\sqrt{1+|\mathbf{x}|^2}}$ for $\mathbf{X} = (X, Y, Z, W) \in S^3$ with $|\mathbf{X}| = 1$ and for $\mathbf{x} = (x, y, z) \in \mathbb{R}^3$. Let us consider the dynamical system equations

$$\left.\begin{aligned} x' &= P_1(x, y, z), \\ y' &= P_2(x, y, z), \\ z' &= P_3(x, y, z), \end{aligned}\right\} \tag{23}$$

where

$$P_1(x,y,z) = \frac{-nxyz}{y+\rho_\Lambda} + \frac{3\gamma n x^2y^2}{2(y+\rho_\Lambda)} - \frac{3\gamma(\gamma-1)xy}{y+\rho_\Lambda} - 2xz + 3\gamma x^2 y,$$
$$P_2(x,y,z) = nyz - \frac{3\gamma nxy^2}{2} - 3y,$$
$$P_3(x,y,z) = -2z^2 + 3\gamma xyz - 2z.$$

Now, we rewrite the maximum degree terms in P_1, P_2 and P_3 by $\bar{P}_1$, $\bar{P}_2$ and $\bar{P}_3$ respectively as follows:

$$\left.\begin{array}{c} \bar{P}_1(x,y,z) = \frac{3\gamma n x^2y^2}{2(y+\rho_\Lambda)} + 3\gamma x^2 y, \\ \bar{P}_2(x,y,z) = -\frac{3\gamma nxy^2}{2}, \\ \bar{P}_3(x,y,z) = 3\gamma xyz. \end{array}\right\} \tag{24}$$

In terms of X, Y and Z, we express the above polynomials as follows:

$$\left.\begin{array}{c} \bar{P}_1(X,Y,Z) = \frac{3\gamma n X^2Y^2}{2(Y+\rho_\Lambda W)W^3} + \frac{3\gamma X^2Y}{W^3}, \\ \bar{P}_2(X,Y,Z) = -\frac{3\gamma nXY^2}{2W^3}, \\ \bar{P}_3(X,Y,Z) = \frac{3\gamma XYZ}{W^3}. \end{array}\right\} \tag{25}$$

The critical points at infinity for the above polynomial system of degree 3 occur at the points $(X,Y,Z,0)$ on the equator of the Poincaré sphere S^3 where $X^2+Y^2+Z^2=1$ [29] and

$$\left.\begin{array}{c} X\bar{P}_2(X,Y,Z) - Y\bar{P}_1(X,Y,Z) = 0, \\ X\bar{P}_3(X,Y,Z) - Z\bar{P}_1(X,Y,Z) = 0, \\ Y\bar{P}_3(X,Y,Z) - Z\bar{P}_2(X,Y,Z) = 0. \end{array}\right\} \tag{26}$$

Then, we substitute the values of $\bar{P}_1, \bar{P}_2, \bar{P}_3$ in terms of X, Y and Z in the above system of equations. Now, we express the above system of equations (26) in terms of X, Y and Z as follows:

$$\left.\begin{array}{c} X(-\frac{3\gamma nXY^2}{2}) - Y(\frac{3\gamma nX^2Y}{2} + 3\gamma X^2Y) = 0, \\ X(3\gamma XYZ) - Z(\frac{3\gamma nX^2Y}{2} + 3\gamma X^2Y) = 0, \\ Y(3\gamma XYZ) - Z(-\frac{3\gamma nXY^2}{2}) = 0. \end{array}\right\} \tag{27}$$

Noting that $X^2+Y^2+Z^2=1$ must hold on the equator of the Poincaré sphere and solving the above system, we see that the fixed point at infinity occurs at $S(\pm 1,0,0,0)$. The flow defined by the system (23) in a neighbourhood of $S(\pm 1,0,0,0) \in S^3$ is topologically equivalent to the flow defined by the following system:

$$\left.\begin{array}{c} \pm y' = -2nyzw + 3\gamma ny^2 - 3\gamma^2 yw^2 + 6\gamma yw^2 - 2wzy + 2\gamma y^2 w, \\ \pm z' = (2-n)z^2 w + yz(\frac{3\gamma n}{2} - 3\gamma) + (2 - 3\gamma(\gamma-1))zw^2 - 2z^2 w^2 + 3\gamma wyz, \\ \pm w' = -nzw^2 + \frac{3\gamma nwy}{2} - 3\gamma(\gamma-1)w^3 - 2zw^2 + 3\gamma yw^2. \end{array}\right\} \tag{28}$$

It is obvious that $(0,0,0)$ is a non-hyperbolic fixed point of system (28) where the Jacobian matrix at $(0,0,0)$ is a null matrix which has all its eigenvalues as zero. Now, we perturb the system (28) by a small amount taking $y = \eta_y$, $z = \eta_z$ and $w = \eta_w$. By doing this, we can find the perturbation functions along each of the axes as functions of Θ. If the system comes back to the fixed point following the perturbation, then the system is stable, otherwise if the perturbation grows, causing the system to move away from the fixed point, then the system is unstable [34]. Nandan Roy and Narayan Banerjee [34] have also used the concept of a perturbation function to analyze stability for non-hyperbolic fixed points for three dimensional systems where linear stability fails. Analysis using the perturbation function approach is also clearly shown in [6]. Now considering the expression (28) corresponding to $+y$, $+z$ and $+w$ respectively, the expressions of η_y, η_z and η_w become

$$\begin{aligned} \frac{d\eta_y}{d\Theta} &= 3\gamma n\eta_y^2, \\ \Rightarrow \eta_y &= \frac{-1}{3\gamma n\Theta + C_1}. \end{aligned}$$

Similarly, we obtain

$$\begin{aligned} \eta_z &= C_2, \\ \eta_w &= \pm\frac{1}{6\gamma(\gamma-1)\Theta + C_3}, \end{aligned}$$

where C_1, C_2 and C_3 denote the arbitrary constants of integration.

Since all of η_y, η_z and η_w fail to grow as Θ tends to infinity which is shown in Fig. 3, we conclude that the fixed point $S(\pm 1, 0, 0, 0)$ is a stable fixed point. Since in a topologically equivalent system, all the topological properties share the same behavior, we conclude that the fixed point at infinity of the original dynamical system represented by (23) is also a stable fixed point which behaves as a late time attractor and it contributes to the model with an accelerated expansion epoch of the evolving Universe.

We obtain the value of the equation of state parameter for the dark energy sector ω_{de} as follows:

$$\omega_{de} = \frac{p_\Lambda}{\rho_\Lambda}, \tag{29}$$

where $p_\Lambda = \frac{1}{8\pi G}(-2\dot{H} - 3H^2 - \frac{k}{a^2}) - (\gamma-1)\rho_m$ and $\rho_\Lambda = \frac{1}{8\pi G}(3H^2 + \frac{3k}{a^2}) - \rho_m$.

Substituting the value of $\dot{H}$ and necessary substitutions, we obtain $\omega_{de} = -1$ at present time. This indicates that the Universe is associated with purely cosmological constant type dark energy and the present model behaves as a cosmological constant model. In terms of the redshift parameter z_r with the redshift function $a(t) = \frac{1}{1+z_r}$, we obtain the following expressions of the total density parameter Ω_{total}, Hubble parameter H and deceleration parameter q as follows:

$$\Omega_{total} = \Omega_\Lambda + \Omega_m = 1 + z,$$

where the vacuum energy density $\Omega_\Lambda = 1 + z - xy$ and the matter density $\Omega_m = xy$. Now,

$$\Omega_{total} = 1 + \frac{3k(1+z_r)^2}{4\pi D_2 \ln \frac{D_1}{(1+z_r)}}, \tag{30}$$

where D_1 and D_2 are arbitrary constants of integration.

$$H(z_r) = \frac{8\pi d_2}{\{\frac{3k_1}{2}(1+z_r)\}^{\frac{1}{3}}} + \frac{d_3}{24\pi d_2}(\frac{3k_1}{2})^{\frac{2}{3}}(1+z_r)^{\frac{5}{3}}, \tag{31}$$

$$\begin{aligned} q(z_r) = \frac{1}{\frac{8\pi d_2}{\{\frac{3k_1}{2}(1+z_r)\}^{\frac{1}{3}}} + \frac{d_3}{24\pi d_2}(\frac{3k_1}{2})^{\frac{2}{3}}(1+z_r)^{\frac{5}{3}}} \{\frac{-8\pi d_2}{3(\frac{3k_1}{2})^{\frac{1}{3}}}(1+z_r)^{\frac{-1}{3}} \\ + \frac{5d_3}{72\pi d_2}(\frac{3k_1}{2})^{\frac{2}{3}}(1+z_r)^{\frac{5}{3}}\} - 1, \end{aligned} \tag{32}$$

where $k_1 = \frac{8\pi d_2(2-3\gamma)k}{9\gamma}$ and d_2, d_3 are the arbitrary constants of integration.

Also, the value of transition redshift, z_{rt} can be calculated using equation (16). The plot for H with respect to z_r is shown in Fig. 8. From this plot, we see that H is a monotonously increasing function of cosmic time, t and at present where $z_r \to 0$ the present value of H takes $H(z_{ro}) = 71.06$ which agrees with the observational data [35]. At late time, when $z_{rt} \to -1$, the curve tends to infinity which means that the rate of expansion becomes infinitely large. The plot of q against z_r is shown in Fig. 9 and Fig. 10 for $k_1 = \frac{-8\pi d_2(2-3\gamma)}{9\gamma}$ and $k_1 = \frac{8\pi d_2(2-3\gamma)}{9\gamma}$ respectively. The negative value of q signifies there is accelerated expansion in the model universe. We observed from Fig. 9 that the transition from the early deceleration ($q > 0$) into the current accelerated one ($q < 0$) occurs at $z_{rt} = 0.61$ with the value of γ taken as $\gamma > \frac{2}{3}$ so that the constant k_1 remains positive in the expression of H. For $\gamma < \frac{2}{3}$ with positive value of $k_1 = \frac{8\pi d_2(2-3\gamma)}{9\gamma}$ the transition occurs at $z_{rt} = 0.74$ which is clearly seen from Fig. 10. Here, in the case of Model II, we find that the transition takes place at a relatively higher redshift for $\gamma < \frac{2}{3}$ while it tends to occur at a relatively lower redshift for $\gamma > \frac{2}{3}$. Further in this model, $\omega_{de} = -1$ and hence the model represents a purely cosmological constant type dark energy

model. The plot of ω_{de} with respect to z_r is shown in Fig. 11. The fixed points and their nature of stability are shown in Table 1 while the present values of the above cosmological parameters are shown in Table 2. This describes a dark energy model which supports the accelerated expansion phenomena of the Universe.

1.3 Model III-$\dot{G} \neq 0$, $\dot{\rho_\Lambda} \neq 0$:

Motivated by the idea that vacuum energy density ρ_Λ can be time dependent [16], we consider here $\dot{\rho_\Lambda} \neq 0$. As $\dot{G} \neq 0$ and $\dot{\rho_\Lambda} \neq 0$, the relation (4) leads to the following equation [17]:

$$\dot{G}(\rho_m + \rho_\Lambda) + G\dot{\rho_\Lambda} = 0. \tag{33}$$

In order to achieve a possible unification of gravitation and elementary particle physics, there have been many extensions of Einstein's theory of gravitation with time-dependent G and the possibility of increasing G has been observed by assuming $G \propto H^{-1}$ [8]. When the Universe is required to have expansion from a finite minimum volume, the critical density assumption and the conservation of the energy-momentum tensor dictate that G increases in a perpetually expanding Universe [8]. Taking motivation from these results, we assume that G varies with time through H as $G = G_o H^{(-1/m)}$, where G_o, $m \in \mathbb{R}$ are real constants, G_o being the present value of G and $m > 0$. The use of this expression of G will help us in finding H in terms of redshift z_r in a subsequent study. This further paves the way for other cosmological parameters such as q, ω_{de}, etc that would help decide the fate of the future Universe, to be expressed in terms of redshift. This not only allows to analyze the dynamics of the Universe in late time as t tends to infinity, but it also helps us to restrict ourselves within the range $z_r \in [-1, 1]$ to understand and explain the whole dynamics.

Using equations (2), (3), (7) and (33) along with the newly introduced variables x, y, z and ϕ such that $x = \frac{8\pi G}{3H^2}$, $y = \rho_m$, $z = \frac{k}{H^2a^2}$ and $\phi = \rho_\Lambda$, we get the following $ASODE$:

$$x' = -\frac{x^2yz}{m(z+1)} + \frac{3\gamma x^3y^2}{2m(z+1)} - \frac{x^2\phi z}{m(z+1)} + \frac{3\gamma x^3y\phi}{2m(z+1)} + \gamma x^2y - \frac{2xz}{3}, \tag{34}$$

$$y' = -\frac{2z^2}{x} + 3\gamma yz - \frac{2z}{x} - \gamma y(z+1) + \frac{2z(z+1)}{3x}, \tag{35}$$

$$z' = -2z^2 + 3\gamma xyz - 2z, \tag{36}$$

$$\phi' = \frac{1}{m}(yz - \frac{3\gamma xy^2}{2} + \phi z - \frac{3\gamma xy\phi}{2}). \tag{37}$$

Let us note that $z \neq -1$ to analyze the system in a finite phase plane. From equations (34), (35), (36) and (37), it is obvious that $F(b_1, 0, 0, b_2)$ is the fixed point of the above dynamical system, where $b_1 \in \mathbb{R} - \{0\}, b_2 \in \mathbb{R}$ such that $b_1b_2 = 1$. The Jacobian matrix of the above dynamical system at F, J_F is given by:

$$J_F = \begin{pmatrix} 0 & \frac{-3\gamma a^3 b}{2m} + \gamma a^2 & -a^2 b - \frac{2a}{3} & 0 \\ 0 & -\gamma & \frac{-4}{3a} & 0 \\ 0 & 0 & -2 & 0 \\ 0 & \frac{-3\gamma}{2m} & \frac{b}{m} & 0 \end{pmatrix}.$$

The above matrix has four eigenvalues: 0,0,$-\gamma$ and -2. The presence of zero eigenvalues makes F a non-hyperbolic fixed point whose stability can be analysed through perturbation function approach. Let η_x, η_y, η_z and η_ϕ denote the perturbations along x, y, z and ϕ axes respectively. Then from equations (34),(35),(36) and (37), we obtain the following perturbations as functions of logarithmic time Θ:

$$\left.\begin{aligned} \eta_x &= d_{o3}, \\ \eta_y &= d_{o4} e^{-\gamma\Theta}, \\ \eta_z &= d_{o5} e^{-2\Theta}, \\ \eta_\phi &= d_{o6}, \end{aligned}\right\} \tag{38}$$

where d_{o3}, d_{o4}, d_{o5} and d_{o6} are arbitrary constants of integration.

From Fig. 4, we see that the perturbations along each of the axes fail to grow as Θ increases and it either evolves to a constant value or decays to zero as Θ tends to infinity. Hence, F is a stable fixed point. The expressions for $\omega_{de}, \Omega_{total}, H, q$ and z_{rt} are obtained as follows:

$$\omega_{de} = \frac{-z - 1 + xy}{x\phi},$$

$$\Omega_{total} = \Omega_\Lambda + \Omega_m = 1 + z.$$

In terms of the redshift parameter z_{rt} with the redshift function $a(t) = \frac{1}{1+z_r}$, we get the following relations:

$$\omega_{de} = \frac{-(z(z_r) + 1) + x(z_r)y(z_r)}{x(z_r)\phi(z_r)}, \tag{39}$$

where

$$x(z_r) = \tfrac{8\pi G_o}{3}\{D_3 \ln(1 + z_r) + D_4\}^{\frac{-2m-1}{m+1}},$$

$$y(z_r) = D_5 \ln(1 + z_r)^{3\gamma},$$

$$z(z_r) = \frac{k(1+z_r)^2}{\{D_3 \ln(1+z_r)+D_4\}^{\frac{2m}{m+1}}},$$

$$\phi(z_r) = \frac{k(1+z_r)^2 + \{D_3 \ln(1+z_r)+D_4\}^{\frac{2m}{m+1}}}{\frac{8\pi G_o}{3}\{D_3 \ln(1+z_r)+D_4\}^{\frac{-1}{m+1}}} - D_5 \ln(1 + z_r)^{3\gamma}.$$

Now, the expression of the total density parameter Ω_{total}, Hubble parameter H and deceleration parameter q in terms of z_r are as follows:

$$\Omega_{total} = 1 + \frac{k(1 + z_r)^2}{\{D_3 \ln(1 + z_r) + D_4\}^{\frac{2m}{m+1}}}, \tag{40}$$

$$H(z_r) = \begin{cases} D_6\{D_3 \ln(1+z_r) + D_4\}^{\frac{m}{m+1}}, & m = \frac{1}{4n}; \\ D_6\{D_3 \ln(1+z_r) + D_4\}^{\frac{m}{m+1}(-1)^{\frac{4m+1}{2m+1}}}, & m \neq \frac{1}{4n}, \end{cases} \tag{41}$$

$$q(z_r) = \begin{cases} \frac{D_3 m}{m+1}\{D_3 \ln(1+z_r) + D_4\}^{-1} - 1, & m = \frac{1}{4n}; \\ \frac{D_3 m}{m+1}(-1)^{\frac{4m+1}{2m+1}}\{D_3 \ln(1+z_r) + D_4\}^{-1} - 1, & m \neq \frac{1}{4n}, \end{cases} \tag{42}$$

where D_3, D_4, D_5, D_6 are arbitrary constants of integration.

Also, the value of the transition redshift can be calculated using equation (16). The fixed points obtained and their stability nature are summarized in Table 1 and the present values of the parameters evaluated above, that is, H, q, z_{rt} and ω_{de} are noted down in Table 2. Fig. 12 shows the plot for H with respect to z_r and we find that the value of H increases as z_r decreases, that is, H increases with the increase in cosmic time t. At present where $z_r = 0$, we obtain $H(z_{ro}) = 71.13$ which is in consonance with the observational data [35]. At late time, the value of H tends to infinity. Fig. 13 shows the plot of q against z_r where we observe that q evolves from the early decelerated regime and the Universe undergoes a dynamic phase transition from deceleration to acceleration at $z_{rt} = 0.723$. This is true for any arbitrary k. However, the model describes a purely accelerating Universe if $m = \frac{1}{4n}$, $n = 1, 2, 3...$ as supported from Fig. 14 where q remains negative in the entire $[-1, 1]$ interval. Fig. 11 shows the plot for ω_{de} against z_r where it is observed that Model III exhibits a purely cosmological constant type dark energy model with $\omega_{de} = -1$. Hence, the model describes an expanding universe where the expansion is accelerating and thus supports the accelerated expansion phenomena of the current Universe which is in concordance with the observations [35].

2 Testing of model's parameter space

In this section, we match the parameters to known values which are in agreement with observational data to check the compatibility of the model with what is being expected. For this, we shall first set a null hypothesis and then, doing necessary calculations for the given data, we will find the value of χ^2. If the calculated value of $\chi^2(\chi^2(calculated))$ is less than the tabulated value of $\chi^2(\chi^2(tabulated))$, that is, $\chi^2(calculated) < \chi^2(tabulated)$, then we conclude that the discrepancy is insignificant and hence, we can accept the null hypothesis [46]. For instance, let us consider the parameter $H(z_{r_o})$ using (31) for matching with the known values of $H(z_{r_o})$ based on observational data.

For example, consider the present value of $H(z_r)$ denoted by $H(z_{r_o})$ from Model II and set a null hypothesis as follows: Null hypothesis: "The theoretically calculated value of $H(z_{r_o})$ fits well with the observed data."

The number of degrees of freedom, n = number of data collected − number of constraints $= 4-1 = 3$, subject to one linear constraint $(\sum O_i = \sum E_i), i = 1, 2, 3, 4$, where O_i represents the observational data entries and E_i represents theoretically calculated values.

Also the tabulated value of χ^2 for 3 degrees of freedom at 5 percent level of significance, $\chi^2(tabulated)_{0.05}$= 7.815 [46].

With respect to observational data in [35], we collect four data values of $H(z_{r_o})$ and marked as $O_i; i = 1, 2, 3, 4$ as shown in Table 3. Then using (31), we find the values of $H(z_{r_o})$ at different values of constants involved and marked them as $E_i; i = 1, 2, 3, 4$.

Now, χ^2 is expressed as $\chi^2 = \sum \frac{(O_i - E_i)^2}{E_i}$. From Table 3, it is found that the calculated value $\chi^2(calculated) = 0.0108$ which is much less than the tabulated value $\chi^2(tabulated)_{0.05} = 7.815$. So it is highly insignificant and hence, we can accept the null hypothesis at 5 percent level of significance. Hence, we can conclude that there is a good correspondence between the theoretical results and the observational data.

Table 3 shows the matching of evaluated values of $H(z_{ro})$ with known values based on observational data for all of the three models. In the similar way, we show the matching of evaluated values for other cosmological parameters such as $q(z_{ro}), z_{rt}$ and ω_{de} for all of the models in Table 4, Table 5, Table 6 and Table 7 respectively. From the tables it is seen that $\chi^2(calculated) << \chi^2(tabulated)_{0.05}$ and hence, we conclude that the calculated values of the above parameters in all of the three models agree with the observational data at 5 percent level of significance.

Table 1. Fixed points and nature of stability for Model I, Model II and Model III.

Fixed points	Type of fixed point	Eigen-values	ω_{de}	Ω_{total}	Behavior
Model I					
$f_1(\frac{2b}{3}, 0, 0)$, $b = 4\pi G\rho_\Lambda$	non-hyperbolic	0,-3γ,-2		$\Omega_{total} = 1 + \frac{k(1+z_r)^2}{(c_3 + c_4 \ln \frac{1}{1+z_r})^{\frac{2}{3}}} \simeq 1,\ k = 0$	stable, behaves as late-time attractor
Model II					
$F_1(0, 0, 0)$	non-hyperbolic	$0, -3, -2$	$\simeq -1$	$\Omega_{total} = 1 + \frac{3k(1+z_r)^2}{4\pi D_2 \ln \frac{D_1}{(1+z_r)}} \simeq 1,\ k = 0$	stable, behave as late-time attractors
$F_2(0, -3, -2)$	non-hyperbolic	$0, -3, -2$	$\simeq -1$		
$S(\pm 1, 0, 0, 0)$	non-hyperbolic	0, 0, 0	$\simeq -1$		
Model III					
$F(b_1, 00, b_2)$	non-hyperbolic	0,0,$-\gamma$,-2	$\simeq -1$	$\Omega_{total} = 1 + \frac{k(1+z_r)^2}{\{D_3 \ln(1+z_r) + D_4\}^{\frac{2m}{m+1}}} \simeq 1,\ k = 0$	stable, late-time attractor

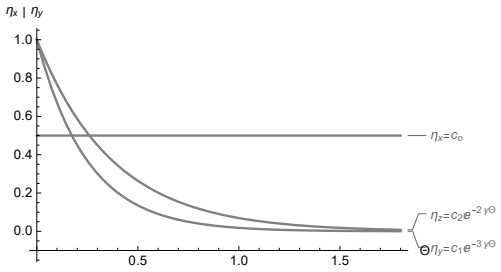

Fig. 1. The figure shows the variation of η_x, η_y, η_z with respect to Θ for f_1 at $c_o = 0.5$, $c_1 = c_2 = 1$, $\gamma = \frac{4}{3}$.

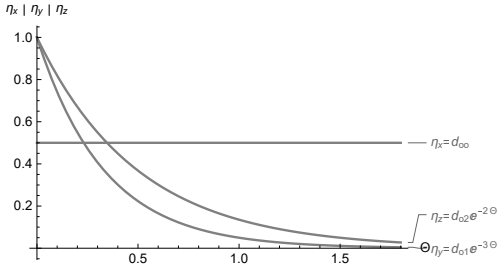

Fig. 2. The figure shows the variation of η_x, η_y and η_z with respect to Θ for F_2 at $d_{oo} = 0.5$, $d_{o1} = d_{o2} = 1$.

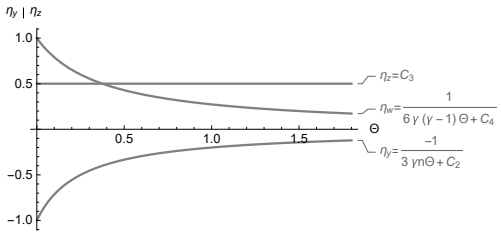

Fig. 3. The figure shows the variation of η_y, η_z, η_w with respect to Θ for fixed point at infinity $S(\pm 1, 0, 0, 0)$ with $C_3 = 0.5, \gamma = \frac{4}{3}, C_2 = C_4 = 1$.

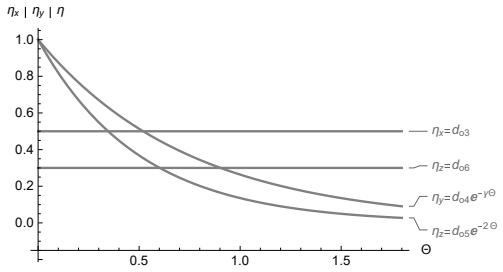

Fig. 4. The figure shows the variation of η_x, η_y, η_z with respect to Θ for F at $d_{o3} = 0.5, d_{o4} = d_{o5} = 1, d_{o6} = 0.3$, $\gamma = \frac{4}{3}$.

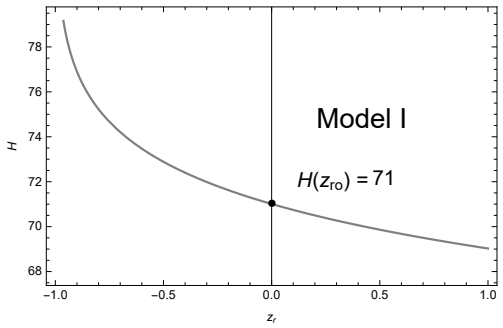

Fig. 5. The figure shows the graphical behavior of $H(z_r)$ in redshift for Model I at $c_1 = 1207, c_2 = 4999$.

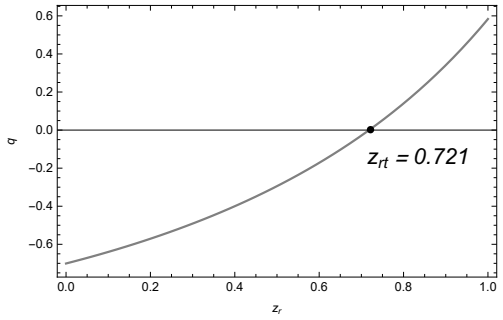

Fig. 6. The figure shows the graphical behavior of $q(z_r)$ in redshift for Model I at $c_2 = 3.06$.

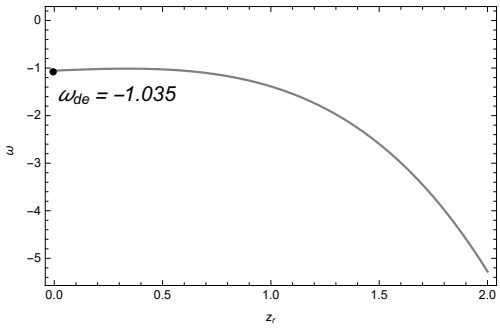

Fig. 7. The figure shows the graphical behavior of ω_{de} in redshift for Model I at $k = -1$: $c_3 = 10, c_4 = 1, c_5 = -0.8, \Lambda_o = 5.3566 \times 10^{-10}, \alpha_2 = 0.26, \alpha_4 = 0.46, \gamma = \frac{4}{3}$; $k = 1 : c_3 = 2, c_4 = 1, \Lambda_o = 5.3566 \times 10^{-10}, \alpha_2 = 2.26, \alpha_4 = 0.48, \gamma = \frac{2}{3}$.

]

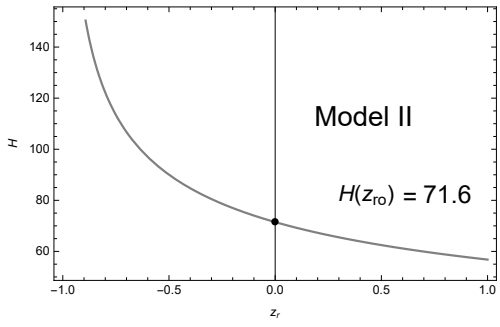

Fig. 8. The figure shows the graphical behavior of $H(z_r)$ in redshift for Model II at $k = -1$: $d_2 = 0.0043, d_3 = 1$; $k = 1 : d_2 = 11.75, d_3 = 1$, $\gamma = \frac{4}{3}$.

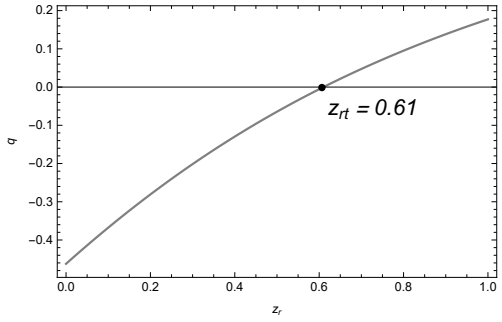

Fig. 9. The figure shows the graphical behavior of $q(z_r)$ in redshift for Model II at $k = -1, d_2 = 0.0043, d_3 = 1, \gamma = \frac{4}{3}$.

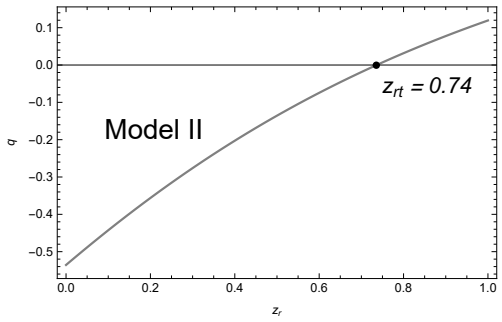

Fig. 10. The figure shows the plot of q against z_r for Model II at $k = 1, d_2 = 0.01, d_3 = 1, \gamma = \frac{1}{3}$.

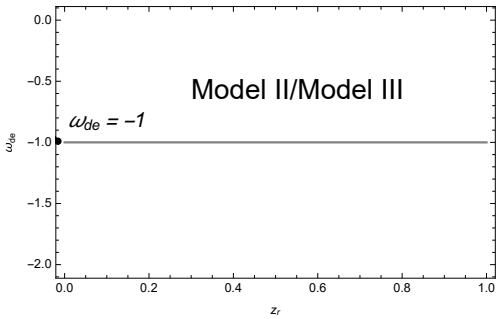

Fig. 11. The figure shows the plot of ω_{de} in redshift for Model II and Model III.

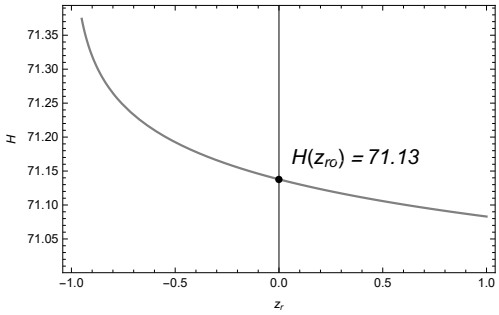

Fig. 12. The figure shows the graphical behavior of $H(z_r)$ in redshift for Model III at $\gamma = \frac{4}{3}, d_2 = 0.0043, d_3 = 1, m = \frac{1}{2}$.

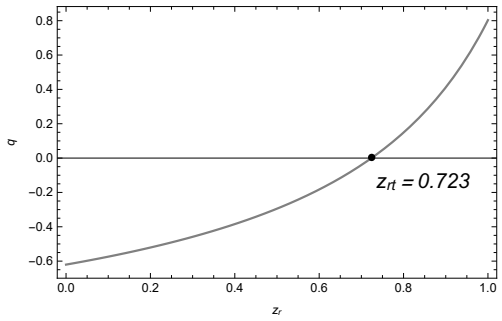

Fig. 13. The figure shows the graphical behavior of $q(z_r)$ in redshift for Model III at $D_3 = 1, D_4 = -0.878, m = \frac{1}{2}$.

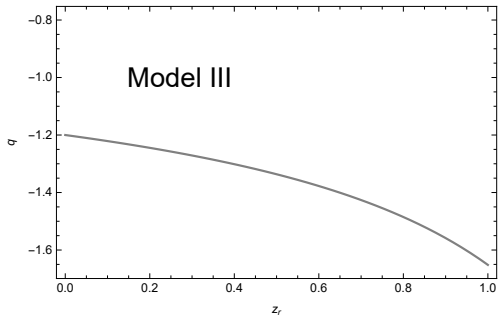

Fig. 14. The figure shows the purely accelerating behavior of q against z_r for Model III at $m = \frac{1}{4}, D_3 = 1, D_4 = -0.878$.

Table 2. Present values of cosmological parameters.

EoS Parameter	Model I	Model II	Model III	Observations
$H(z_{ro})$	71.00, $c_1 = 1207$, $c_2 = 4999$	71.6, $(k = 1 : d_2 = 17$, $d_3 = 1, \gamma = \frac{1}{3})/$ $(k = -1 : \gamma = \frac{4}{3}$, $d_3 = 1, d_2 = 12.05)$	71.13, $D_3 = -1199$, $D_4 = 359999$, $m = \frac{1}{2}$	73 ± 1.4 [32]
$q(z_{ro})$	-0.70 $c_2 = 3.06$	-0.46 $(k = -1, \gamma = \frac{4}{3}$, $d_2 = 0.0043, d_3 = 1)$ -0.54 $(k = 1, \gamma = \frac{1}{3}$, $d_2 = 0.01, d_3 = 1)$	-0.72 $(D_3 = 2$, $D_4 = 0.42$, $m = \frac{1}{2})$	-1.08 ± 0.29 [9]
z_{rt}	0.721 $c_2 = 3.045$	0.61, $(k = -1, \gamma = \frac{4}{3}$, $d_2 = 0.0043, d_3 = 1)$ 0.74 $(k = 1, \gamma = \frac{1}{3}$, $d_2 = 0.01, d_3 = 1)$	0.716 $(D_3 = 2$, $D_4 = 0.42$, $m = \frac{1}{2})$	0.61 $(k = 1)$, $0.73(k = -1)$ [13] $0.72(k = 0$, Λ CDM) [31]
$\omega_{de}(z_{ro})$	-1.03571 $(k = -1 : C_5 = -8.7$, $\alpha_2 = 2, \alpha_4 = 6.4)$; $(k = 1 : C_5 = 0.625$, $\alpha_2 = 3.49, \alpha_4 = 2.9)$, $\Lambda_o = 5.3566 \times 10^{-10}$, $C_3 = C_4 = 1, \gamma = \frac{4}{3}$	-1	-1	-1.03 ± 0.03 [25]

Table 3. Matching the predicted value of $H(z_{ro})$ against the observational data.

Known value	Theoretically calculated value	Model I	Model II	Model III
(O_i) (from observational data in [35])	(Model I, Model II, Model III) $(E_{1i},\ E_{2i},\ E_{3i})$, $i = 1, 2, 3, 4.$	$\chi^2_{1i}=\frac{(O_i-E_{1i})^2}{E_{1i}}$	$\chi^2_{2i}=\frac{(O_i-E_{2i})^2}{E_{2i}}$	$\chi^2_{3i}=\frac{(O_i-E_{3i})^2}{E_{3i}}$
66.88	(71, 67.1, 71.02) for $(E_{11} : c_1 = 1207, c_2 = 4999)$; $(E_{21} : k = 1, d_2 = 31.04, \gamma = \frac{1}{3}$; $k = -1, d_2 = 59.75, \gamma = \frac{4}{3}$, $d_3 = 1)$; $(E_{31} : D_3 = -1199$, $D_4 = 357911, m = \frac{1}{2})$	0.2390	0.0007	0.2413
68.44	(66.42, 68.0, 68.88) for $(E_{12} : c_1 = 1060, c_2 = 4990)$; $(E_{22} : k = 1, d_2 = 31.89, \gamma = \frac{1}{3}$; $k = -1, d_2 = 61.37, \gamma = \frac{4}{3}$, $d_3 = 1)$; $(E_{32} : D_3 = -1000$, $D_4 = 326798, m = \frac{1}{2})$.	0.0614	0.0029	0.0028
69.90	(68.90, 70.5, 66.00) for $(E_{13} : c_1 = 1140.8, c_2 = 4900)$; $(E_{23} : k = 1, d_2 = 34.28, \gamma = \frac{1}{3}$; $k = -1, d_2 = 65.96, \gamma = \frac{4}{3}$, $d_3 = 1)$;$(E_{33} : D_3 = -1190$, $D_4 = 287496, m = \frac{1}{2})$.	0.0145	0.0051	0.2304
67.66	(66.36, 67.28, 66.78) for $(E_{14} : c_1 = 1058.3, c_2 = 4900)$; $(E_{24} : k = 1, d_2 = 31.22, \gamma = \frac{1}{3}$; $k = -1, d_2 = 60.08, \gamma = \frac{4}{3}$, $d_3 = 1)$; $(E_{34} : D_3 = -1199$, $D_4 = 297809, m = \frac{1}{2})$.	0.0254	0.0022	0.0115
$\sum_{i=1}^{4} O_i$ $=272.88$	$\sum_{i=1}^{4} E_{1i} = \sum_{i=1}^{4} E_{2i} = \sum_{i=1}^{4} E_{3i}$ $=272.88$	$\chi^2 = \sum_{i=1}^{4} \chi^2_{1i}$ $=0.3403$	$\chi^2 = \sum_{i=1}^{4} \chi^2_{2i}$ $=0.0108$	$\chi^2 = \sum_{i=1}^{4} \chi^2_{3i}$ $=0.4860$

Table 4. Matching the predicted value of $q(z_{ro})$ against values known from observations.

Known value $-q(z_{ro}) = O_i$,	Theoretically calculated value $-q(z_{ro}) = E_{ji}$, $j = 1, 2, 3, i = 1, 2, 3, 4.$ (Model I, Model II, Model III) (E_{1i}, E_{2i}, E_{3i}), $i = 1, 2, 3, 4.$	Model I $\chi^2_{1i} = \frac{(O_i - E_{1i})^2}{E_{1i}}$	Model II $\chi^2_{2i} = \frac{(O_i - E_{2i})^2}{E_{2i}}$	Model III $\chi^2_{3i} = \frac{(O_i - E_{3i})^2}{E_{3i}}$
0.5978 [4]	(0.620,0.690,0.67) for $(E_{11} : c_2 = 2.50)$; $(E_{21} : k = 1, d_2 = -0.00150;$ $k = -1, d_2 = -0.001263, d_3 = 1)$; $(E_{31} : m = \frac{1}{2}, D_3 = 1,$ $D_4 = -1.014)$	0.00079	0.01449	0.00778
0.5200 [6]	(0.690,0.540,0.60) for $(E_{12:c_2=3.00})$; $(E_{22} : k = 1, d_2 = -0.00196;$ $k = -1, d_2 = -0.00098, d_3 = 1)$; $(E_{32} : m = \frac{1}{2}, D_3 = 1,$ $D_4 = -0.800)$	0.04188	0.00074	0.01067
0.53024 [4]	(0.450,0.460,0.500) for $(E_{13:c_2=2.00})$; $(E_{23} : k = 1, d_2 = -0.00162;$ $k = -1, d_2 = -0.000812, d_3 = 1)$; $(E_{33} : m = \frac{1}{2}, D_3 = 1,$ $D_4 = -0.70)$	0.01431	0.02630	0.00183
0.65100 [6]	(0.69,0.62,0.64) for $(E_{14} = c_2 = 2.79)$; $(E_{24} : k = 1, d_2 = -0.00228;$ $k = -1, d_2 = -0.00124, d_3 = 1)$; $(E_{34} : m = \frac{1}{2}, D_3 = 1,$ $D_4 = -0.921)$	0.00220	0.00145	0.00019
$\sum_{i=1}^{4} O_i$=2.3,	$\sum_{i=1}^{4} E_{ji}$=2.3,	$\sum_{i=1}^{4} \chi^2_{1i}$ = 0.05918	$\sum_{i=1}^{4} \chi^2_{2i}$ =0.04298	$\chi^2 = \sum_{i=1}^{4} \chi^2_{3i}$, =0.02047

Table 5. Matching the predicted value of z_{rt} from Model II against values known from observations.

Known value of z_{rt} (O_i), $i = 1, 2, 3, 4$ from [13]	Theoretical value of z_{rt} (E_i), $i = 1, 2, 3, 4$ at $\gamma = \frac{4}{3}$	$(O_i - E_i)^2$	$\frac{(O_i - E_i)^2}{E_i}$
0.45	0.46 at $k = -1$, $d_2 = 0.00354$, $d_3 = 1$	0.0001	0.00022
0.49	0.45 at $k = -1$, $d_2 = 0.00348$, $d_3 = 1$	0.0016	0.00360
0.55	0.61 at $k = -1$, $d_2 = 0.00429$, $d_3 = 1$	0.0036	0.0059
0.61	0.58 at $k = -1$, $d_2 = 0.00414$, $d_3 = 1$	0.0009	0.0016
$\sum O_i$=2.1	$\sum E_i$=2.1		$\chi^2 = \sum \frac{(O_i - E_i)^2}{E_i}$ =0.011
0.59	0.55 at $k = 1, d_2 = 0.00797$, $d_3 = 1$, $\gamma = \frac{1}{3}$	0.0016	0.00291
0.62	0.66 at $k = 1, d_2 = 0.00914$, $d_3 = 1$, $\gamma = \frac{1}{3}$	0.0016	0.00242
0.65	0.74 at $k = 1, d_2 = 0.01004$, $d_3 = 1$, $\gamma = \frac{1}{3}$	0.0081	0.01095
0.73	0.64 at $k = 1, d_2 = 0.00892$, $d_3 = 1$, $\gamma = \frac{1}{3}$	0.0081	0.01266
$\sum O_i$=2.59	$\sum E_i$=2.59		$\chi^2 = \sum \frac{(O_i - E_i)^2}{E_i}$ =0.029

Table 6. Matching the predicted value of ω_{de} at present time against values known from observation.

Known value	Theoretically calculated value	Model I	Model II	Model III
$-\omega_{de} = O_i$	$-\omega_{de} = E_{ji}$ (Model I, Model II,Model III) $(E_{1i},\ E_{2i},\ E_{3i})$ $j = 1, 2, 3,$ $i = 1, 2, 3, 4.$	χ^2_{1i}=$\frac{(O_i - E_{1i})^2}{E_{1i}}$	χ^2_{2i}=$\frac{(O_i - E_{2i})^2}{E_{2i}}$	χ^2_{3i}=$\frac{(O_i - E_{3i})^2}{E_{3i}}$
1.029 [6]	(1.035, 1, 1) for E_{11} : $(k = -1, \alpha_2 = 0.26,$ $\alpha_4 = 0.46, c_3 = 10,$ $c_4 = 1, c_5 = -0.58);$ $(k = 1, \alpha_2 = 2.26, \alpha_4 = 0.48$ $c_3 = 2, c_4 = 1, c_5 = 2.798),$ $\Lambda_o = 5.0356 \times 10^{-10}, \gamma = 4/3$	0.00004	0.00084	0.00084
1.060 [6]	(1.033, 1, 1) for E_{12} : $(k = -1, \alpha_2 = 0.26,$ $\alpha_4 = 0.46, c_3 = 10,$ $c_4 = 1, c_5 = -0.56);$ $(k = 1, \alpha_2 = 2.26, \alpha_4 = 0.48$ $c_3 = 2, c_4 = 1, c_5 = 2.806,$ $\Lambda_o = 5.0356 \times 10^{-10}, \gamma = 4/3$	0.00071	0.00360	0.00360
1.030 [25]	(1.020, 1, 1) for E_{13} : $(k = -1, \alpha_2 = 0.26,$ $\alpha_4 = 0.46, c_3 = 10,$ $c_4 = 1, c_5 = -0.42);$ $(k = 1, \alpha_2 = 2.26, \alpha_4 = 0.48$ $c_3 = 2, c_4 = 1, c_5 = 2.869,$ $\Lambda_o = 5.0356 \times 10^{-10}, \gamma = 4/3$	0.00009	0.00090	0.00090
1.003 [31]	(1.030, 1, 1) for E_{14} : $(k = -1, \alpha_2 = 0.26,$ $\alpha_4 = 0.46, c_3 = 10,$ $c_4 = 1, c_5 = -0.528);$ $(k = 1, \alpha_2 = 2.26, \alpha_4 = 0.48$ $c_3 = 2, c_4 = 1, c_5 = 2.821,$ $\Lambda_o = 5.0356 \times 10^{-10}, \gamma = 4/3$	0.00071	0.000009	0.000009
$\sum_{i=1}^{4} O_i$ $= 4.1 \simeq 4$	$\sum_{i=1}^{4} E_{1i} = 4.1 \simeq 4,$ $\sum_{i=1}^{4} E_{2i} = \sum_{i=1}^{4} E_{3i}$ $=4$	$\chi^2 = \sum_{i=1}^{4} \chi^2_{1i}$ $=0.00236$	$\chi^2 = \sum_{i=1}^{4} \chi^2_{2i}$ $=0.005349$	$\chi^2 = \sum_{i=1}^{4} \chi^2_{3i}$ $=0.005349$

3 Conclusion

In this paper, we have presented an $FLRW$ cosmological model using dynamical system analysis in spacetimes of arbitrary spacial curvature k. With k we extend the system to a three dimensional dynamical one which is a more generalized way to analyze the dynamical behavior of the Universe. Here we have discussed three models. In model I where both G and ρ_Λ are constants, we obtain one non-hyperbolic fixed point $f_1(\frac{2b}{3}, 0, 0), b = 4\pi G\rho_\Lambda$ which behaves as a stable attractor at late time. In Model II where $\dot{G} \neq 0$, we get two stable fixed points $F_1(0, 0, 0)$, $F_2(\frac{1}{\rho_\Lambda}, 0, 0)$ in finite phase plane and we also analyze stability for fixed points at infinity where the fixed points at infinity lie on the north pole of the Pontcaré sphere S^3 represented by the point $S(\pm 1, 0, 0, 0)$. In Model III, we get a stable fixed point $F(b_1, 0, 0, b_2)$ where $b_1 \in \mathbb{R} - \{0\}, b_2 \in \mathbb{R}$ such that $b_1 b_2 = 1$. The fixed points for all of the three models and their nature of stability have been tabulated in Table 1. The cosmological parameters such as the Hubble parameter $H(z_r)$, deceleration parameter $q(z_r)$, transition redshift z_{rt} and EOS parameter for the dark energy sector ω_{de} are expressed in terms of redshift z_r for all the three models. The present values of these parameters are noted down in Table 2 and they are all in agreement with the observational data [9, 13, 25, 31, 32]. For Model I we get the present values as $H(Z_{ro}) = 71, q(z_{ro}) = -0.70, z_{rt} = 0.723, \omega_{de}(z_{ro}) = -1.03571$. For Model II we get $H(Z_{ro}) = 71.06$, $q(z_{ro}) \simeq -0.5$, $z_{rt} = 0.61$ at $k = -1$, $z_{rt} = 0.74$ at $k = 1$ and $\omega_{de}(z_{ro}) = -1$. For Model III, we have $H(Z_{ro}) = 71.02$, $q(z_{ro}) = -0.72$, $z_{rt} = 0.716$, $\omega_{de}(z_{ro}) = -1$. We find that in Model I, ω_{de} evolves from a phantom region and approaches the value $\omega_{de} \simeq$-1.03571 as $z_r \to 0$ at present which is also graphically depicted in Fig. 14. Thus Model I shows effective phantom behavior while Model II and Model III represent purely cosmological constant type dark energy models with $\omega_{de} = -1$ at present for any arbitrary k as shown in Fig. 16. It is also vividly seen in Fig. 9, Fig. 10, Fig. 11 and Fig. 12 that the value of the deceleration parameter q in each of the three models remains negative in $z \in [-1, 0]$, that is, at present as well as at late times. This behavior shows that the models describe the accelerating Universe. Moreover, the monotonously increasing nature of H with respect to cosmic time as shown in Fig. 5, Fig. 6, Fig. 7 and Fig. 8 indicates that the rate of expansion becomes infinite at late time and this is true for all of the three models. From the value of $\omega_{de} \simeq -1$ that is obtained in each of the three models, we conclude that there is negative pressure in the evolving Universe and the presence of this negative pressure assures that our models: Model I, Model II and Model III represent dark energy models that describe the accelerated expansion epoch of the evolving Universe. It is observed that the cosmological parameters fit well with the observational data in all the three models. However for Model II the transition from early deceleration to current acceleration tends to occur at a slightly lower redshift (later in time) for $k = -1$ while at a slightly higher redshift (earlier in time) for $k = 1$. The estimated values of $H(z_{ro})$, $q(z_{ro})$, z_{rt} and ω_{de} are matched with the values known from observational data and they are shown in Table 3, Table 4, Table 5, Table 6 and Table 7 respectively. The calculated value of χ^2 is found to be less than the tabulated value of χ^2 for each of the parameters which depicts

that the theoretically calculated values of $H_{z_{ro}}$, $q(z_{ro})$, z_{rt} and ω_{de} fit well with the observational data. Hence, there is a good correspondence between our theoretical findings and the observational data. All the three models support the accelerated expansion phenomena of the evolving Universe and the Universe will continue to expand with acceleration at late time as cosmic time t tends to infinity.

Acknowledgements

We are grateful to the anonymous Referees for the detailed revision of our work and for providing useful suggestions which help us a lot to improve the presentation of our results.

Declaration

The authors declare that there is no conflict of interest regarding the publication of this paper.

References

1) A. De Felice and S. Tsujikawa, 2010, *Living Rev. Relativity*, Vol. 13, p. 1-161.
2) A. G. Riess *et al.*, 1998, *Astron. J.* , Vol. 116, p. 1009-1038.
3) Aleksander Stachowski, Marek Szydtowski, 2016, *Eur. Phys. J. C*, Vol. 76, p. 1-21.
4) Anirudh Pradhan, Gopikant K. Goswami, R. Rani, Aroonkumar Beesham, 2023, *Astronomy and Computing*, Vol. 44, p. 100737(1-20).
5) C. Brans and R. H. Dicke, 1961, *Phys. Rev.* , Vol. 124, p. 925-935.
6) Chingtham Sonia and S. Surendra Singh, 2022, *Eur. Phys. J. C*, Vol. 82, p. 863(1-27).
7) C. L. Benett *et al.*, 2003, *Astrophys. J. Suppl.* Vol. 148, p. 119-134.
8) C. P. Singh, 2006, International Journal of Theoretical Physics, Vol. 45, No. 3, p. 531-540.
9) D. Camarena *et al.*, 2020, *Phys. Rev. Res.*, Vol. 2, p. 013028(1-8).
10) D. N. Spergel *et al.*, 2003, *Astrophys. J. Suppl.*, Vol. 148, p. 175-194.
11) D. J. Eisenstein *et al.*, , 2005, *Astrophys. J.* , Vol. 633, p. 560-574.
12) E. L. D. Perico, J. A. S. Lima, Spyros Basilakos, and Joan Solà, 2013, *Phys. Rev. D*, Vol. 88, p. 063531(1-14).
13) Espana-Bonet, C. *et al.* (2004), Testing the running of the cosmological constant with type Ia supernovae at high z, JCAP **2004**(02),006, 1-51.
14) E. Teller, 1948, *Phys. Rev.* , Vol. 73, p. 801-802.
15) G. Cognola, E. Elizalde, S. Nojiri, S. D. Odintsov, L. Sebastiani, and S. Zerbini, 2008, *Phys. Rev. D*, Vol. 77, 046009(1-11).
16) H. Fritzsch, 2015, *Modern Physics Letters A*, Vol. 30, p. 1540034(1-16).
17) Harald Fritzsch, 2012, *Class.Quant.Grav.*, Vol. 29, p. 215002.
18) Ilya L. Shapiro, 2008, *Class. Quantum Grav.* Vol. 25, p. 103001(1-47).
19) I.L. Shapiro, J. Solá, 2002, *JHEP*, Vol. 02, p. 1-28.
20) I.L. Shapiro, J. Solá, 2009, *Phys. Lett. B* , Vol. 682, p. 105-113.
21) J. A. S. Lima and J. M. F. Maia, 1994, *Phys. Rev. D*, Vol. 49, p. 5597-5600.
22) J. A. S. Lima and M. Trodden , 1996, *Phys. Rev. D*, Vol. 53, p. 4280-4286.
23) J. A. S. Lima, E. L. D. Perico, G. J. M. Zilioti, 2015, *International Journal of Modern Physics D*, Vol. 24, p. 1541006(1-16).
24) J. A. S. Lima, Spyros Basilakos, Joan Sola, 2015, *Gen Relativ Gravit.*, Vol. 2015, p. 1-15.
25) J. A. S. Lima, S. Basilakos, J. Solà, 2013, *Monthly Notices of the Royal Astronomical Society*, Vol. 431, p. 923–929.

26) J. C. Carvalho, J. A. S. Lima, and I. Waga, 1992, *Phys. Rev. D*, Vol. 46, 2404-2407.
27) Joan Solá, 2008, *J. Phys. A: Math. Theor.* Vol. 41, p. 164066(1-12).
28) Joan Solà, 2011, *J. Phys.: Conf. Ser.*, Vol. 283, p. 012033(1-14).
29) L. Perko, 1996 , *Texts in applied Mathematics*, Vol. 7.
30) Mavromatos, N.E., Solà Peracaula, J., 2021, *Eur. Phys. J. Spec. Top.*, Vol. 230, 2077–2110.
31) Mehdi Rezaei, Mohammad Malekjani, Joan Solà Peracaula, 2019, *Phys. Rev. D*, Vol. 100, p. 023539(1-19).
32) M. J. Reid *et al.*, 2019, *Astrophys. J. Lett.*, Vol. 886, L27.
33) M. Fierz, Helv., 1956, *Phys. Acta*, Vol. 29, p. 128-134.
34) Nandan Roy and Narayan Banerjee, 2017, *Physical Review D* , Vol. 95, p. 064048(1-12).
35) N. Aghanim *et al.*, 2020, *Astronomy & Astrophysics*, Vol. 641, p. 1-43.
36) Sudipto Roy and Mohsin Islam, 2016 , *International Journal of Physics and Mathematical Sciences*, Vol. 6, p. 1-10.
37) P. Jordan, Schwerkraft and Weltall, 1955, *Grundlagen der theoretischen Kosmologie*, p. 10-17.
38) R. H. Dicke, 1962, *Phys. Rev.*, Vol. 125, p. 2163-2167.
39) R. H. Dicke, 1957, *Rev. Mod. Phys.*, Vol. 29, p. 363-376.
40) R. H. Dicke, 1961, *Nature*, Vol. 192, p. 440-441.
41) Sebastian Bahamonde, Mihai Marciu, Prabir Rudra, 2019, *Physical Rev. D* , Vol. 100, p. 083511(1-14).
42) Roland K.W. Roeder, 2003, Rocky Mountain Journal of Mathematics, Vol. 33, p. 1057-1082.
43) R. R. Caldwell, M. Doran, 2004, *Phys. Rev. D* , Vol. 69, p. 103517(1-6).
44) Samaddar, A., Singh, S.S., 2023, *Gen Relativ Gravit* ,Vol. 55, p. 111.
45) S. Capozziello, R. D. Agostino, and O. Luongo, 2019, *Int. J. Mod. Phys. D* , Vol. 28, p. 1930016(1-81).
46) S. C. Gupta, V. K. Kapoor, 2020, Fundamentals of mathematical statistics, 12^{th} Edition, Sultan Chand and Sons.
47) S. M. Carroll, V. Duvvuri, M. Trodden, and M. S. Turner, 2004, *Phys. Rev. D*, Vol. 70, p. 043528(1-5).
48) S. Nojiri, S. D. Odintsov, and V. K. Oikonomou, 2017, *Phys. Rep.* , Vol. 692, p. 1-104.
49) S. Nojiri and S. D. Odintsov, 2007, *Int. J. Geom. Methods Mod. Phys.*, Vol. 04, p. 115-145.
50) S. Nojiri, S. D. Odintsov, and V. K. Oihonomou, 2017, *Phys. Rep.*, Vol. 692, p. 1-104.
51) Solà Peracaula, J., Yu, H., 2020, *Gen Relativ Gravit* Vol. 52, p. 1-57.
52) S. Perlmutter *et al.* , 1999, *Astrophys. J.*, Vol. 517, p. 565-586.
53) Spyros Basilakos, 2009, *Monthly Notices of the Royal Astronomical Society*, Vol. 395, p. 2347–2355.
54) Spyros Basilakos, Nick E. Mavromatos, Joan Solà Peracaula, 2020, *Phys. Rev. D*, Vol. 101, p. 045001(1-36).
55) S. Rathore, S. Surendra Singh, 2023, *Sci Rep*, Vol. 13, p. 13980(1-13).
56) S. Surendra Singh and Chingtham Sonia, 2020, Vol. 2020, p. 1805350(1-18).
57) T. Clifton, P. G. Ferreira, A. Padilla, and C. Skordis, 2012, *Phys. Rep.*, Vol. 513, 1-189.
58) W. J. Percival *et al.*, 2010, *Mon. Not. R. Astron. Soc.*, Vol. 401, p. 2148-2168.
59) Z. Y. Huang *et al.*, 2006, *JCAP*, Vol. 0605, p. 013(1-10).